Communication

Mode Selection Method Suitable for Dual Circular Polarized OAM Transmission

Kazunori YURI, *Non-Member*, Naoki HONMA and Kentaro MURATA, *Member, IEEE*

***Abstract*—This paper proposes an analog orbital angular momentum (OAM) transmission method based on dual circular polarization (CP), where the low-gain modes are excluded for enhancing the achievable data-rate. Two sequential arrays, each of which has four circular microstrip antennas with dual CP, are used at both transmitter and receiver sides, and face each other. A discrete Fourier transform (DFT) feed network is used at both sides to realize quasi-eigenmode transmission, where mode orthogonalization is achieved by using just an analog circuit; digital interference cancellation is not used. The key idea of the proposed method is its mode selection technique, which simply choses some of the highest modes and distributes all available power to the chosen modes equally. An analysis shows that this method increases the achievable rate by 2 bits/s/Hz compared to short-range multiple input and multiple output (SR-MIMO) when the number of the ports at each side is 8 and the distance between transmitter and receiver antennas is $10\lambda_0$ (λ_0 is wavelength in vacuum) or more. Also, it is found that the achievable rate of the proposed scheme is asymptotic to that of SR-MIMO with water-filling.**

***Index Terms*—discrete Fourier transforms (DFT), eigenmode transmission, orbital angular momentum (OAM), dual circular polarized wave, microstrip antenna**

I. Introduction

Recently, due to the spread of the Internet, demands for higher data-rates continue to grow, even in wireless communication services. Orbital angular momentum (OAM) is attracting significant attention because it can, where the transmitter and receiver antennas are in line of sight (LOS), enhance the data-rate just by increasing the number of the modes, [1] [2] [3]. The OAM scheme using array antennas can be recognized as a kind of short-range (SR) multiple-input and multiple-output (MIMO) communication [4] [5]. A key feature of OAM is the way in which it generates modes, that is, the generated field distribution rotates moment by moment. This feature makes the fixed analog mode generator applicable to OAM transmission because the excitation weight can be easily generated by using a discrete Fourier transform (DFT) feed network [6] [7] [8]. In the analog OAM transmission scheme, the channel between the transmitter and receiver antennas is orthogonalized by the fixed analog feed network, and the signals are transmitted in parallel without any digital interference cancellation. In addition, we use the dual-circular polarizations to improve the data-rate [9] [10] [11]. If the channels of the dual-circular polarizations are completely isolated, i.e., there is no interference between two polarizations, the data-rate can be simply doubled.

Kazunori YURI and Naoki HONMA are with the graduate school of Arts and Science, Iwate University, Morioka, 020-8551 Japan.(e-mail:g0317155@iwate-u.ac.jp)

Kentaro MURATA is with National Defense Academy, Yokosuka 239-0811, Japan.

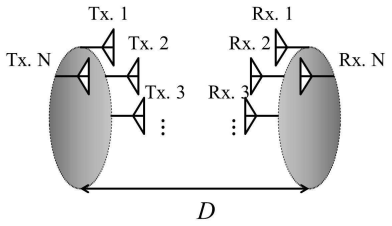

Fig. 1. OAM transmission scheme using circular array antennas.

However, the gain of the all parallel channels is not identical, and some of the modes suffer from the serious degradation of the channel gain. Furthermore, the imperfect channels created by displacement of the antennas cause inter-mode interference and this deteriorates the data-rate. This drawback cannot be overcome, even by increasing the number of antennas.

This paper proposes a simple mode selection scheme suitable for OAM transmission with a fixed analog feed network. Several of the lowest gain channels are excluded from OAM transmission, and all transmission power is equally distributed to the remaining modes. This simple procedure significantly improves the transmission efficiency and inter-mode interference. Numerical simulations are performed to verify the performance of the proposed scheme, where dual-circular polarized microstrip arrays are used at both transmitter and receiver sides. In the remainder of this paper, basic explanations of OAM with array antennas and DFT feed networks are presented for better understanding of the proposed scheme. Also, numerical results are shown to demonstrate the validity of the proposed scheme.

II. Theory

A. Analog OAM transmission

This section reviews the basic idea of the analog OAM transmission method [8] for easier understanding of the method proposed in the next section. Figure 1 shows the system model of OAM transmission using array antennas. The transmitter and receiver antennas are identical in number and

face each other. Channel matrix $\boldsymbol{H}$ is given by

$$\begin{aligned}\boldsymbol{H} &= \begin{pmatrix} h_{1,1} & h_{1,2} & \dots & h_{1,N} \\ h_{2,1} & h_{2,2} & \dots & h_{2,N} \\ \vdots & \vdots & \ddots & \vdots \\ h_{N,1} & h_{N,2} & \dots & h_{N,N} \end{pmatrix} \\ &= \begin{pmatrix} a_{1,1} & a_{1,2} & \dots & a_{1,N} \\ a_{1,N} & a_{1,1} & \dots & a_{1,N-1} \\ \vdots & \vdots & \ddots & \vdots \\ a_{1,2} & \dots & a_{1,N} & a_{1,1} \end{pmatrix}, \end{aligned} \tag{1}$$

where N is the number of transmitting and receiving antenna elements. $\boldsymbol{H}$ becomes a cyclic matrix due to this configuration. Note that the channel is assumed to be ideal, i.e. the remainder of this section assumes the perfect cyclic matrix. In this case, the DFT matrix is completely equivalent to the eigenvector matrix of $\boldsymbol{H}$. Similar to singular value decomposition, the channel can be decomposed as,

$$\boldsymbol{H} = \boldsymbol{W}_N \boldsymbol{C} \boldsymbol{W}_N^H, \tag{2}$$

where $\boldsymbol{W}_N$ is a unitary DFT matrix whose number of elements is N; $\{\cdot\}^H$ is complex conjugate transposition. $\boldsymbol{C}$ becomes a diagonal matrix, which is written as $\boldsymbol{C} = \mathrm{diag}(c_1, \cdots, c_N)$, where c_k is a complex number corresponding to the complex amplitude of the isolated path.

By multiplying the weights, $\boldsymbol{W}_N$ and $\boldsymbol{W}_N^H$, on transmitter and receiver sides, respectively, the resulting channel matrix, $\boldsymbol{H}'$, is diagonalized as,

$$\begin{aligned}\boldsymbol{H}' &= \boldsymbol{W}_N^H \boldsymbol{H} \boldsymbol{W}_N \\ &= \boldsymbol{C}. \end{aligned} \tag{3}$$

The nth column vector (n is a positive integer up to N) of $\boldsymbol{W}_N$ is given by,

$$\boldsymbol{w}_n = \frac{1}{\sqrt{N}} \begin{pmatrix} {w_n}^0 & {w_n}^1 & \dots & {w_n}^{N-1} \end{pmatrix}^T, \tag{4}$$

where $\{\cdot\}^T$ is transposition. w_n is defined by,

$$w_n = \exp\left(\frac{-j2\pi(n-1)}{N}\right). \tag{5}$$

w_n is the rotation factor. For example, when N is 4, $\boldsymbol{W}_4$ is expressed as,

$$\boldsymbol{W}_4 = \frac{1}{2} \begin{pmatrix} e^0 & e^0 & e^0 & e^0 \\ e^0 & e^{-j\frac{\pi}{2}} & e^{-j\pi} & e^{-j\frac{3\pi}{2}} \\ e^0 & e^{-j\pi} & e^0 & e^{-j\pi} \\ e^0 & e^{-j\frac{3\pi}{2}} & e^{-j\pi} & e^{-j\frac{\pi}{2}} \end{pmatrix}. \tag{6}$$

A feed network, which can generate the weight $\boldsymbol{W}_N$, is defined as an DFT feed network in this paper. This DFT feed network can be realized by combining 180 degree hybrid couplers that are considered as the analog components. Figure 2 shows the 180 degree hybrid coupler and its transmission characteristics. The 180 degree hybrid coupler equally distributes the input power to both output ports, and the output

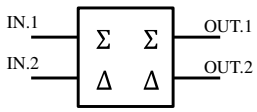

Unit : rad	IN. 1	IN. 2
OUT. 1	0	0
OUT. 2	0	$-\pi$

Fig. 2. 180 degree hybrid coupler.

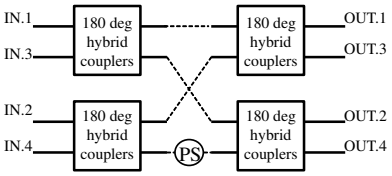

Unit : rad	IN. 1	IN. 2	IN. 3	IN. 4
OUT. 1	0	0	0	0
OUT. 2	0	$-\pi/2$	$-\pi$	$-3\pi/2$
OUT. 3	0	$-\pi$	0	$-\pi$
OUT. 4	0	$-3\pi/2$	$-\pi$	$-\pi/2$

Fig. 3. DFT feed network ($N = 4$).

signals of IN.1 and IN.2 ports are in-phase and anti-phase, respectively. This hybrid circuit can be easily realized by using a rat-race circuit etc.

Figure 3 shows its DFT weight couplers and its transmission characteristics, where N is 4. Four hybrids are combined, and a $-\frac{\pi}{2}$ phase shifter (PS) is used as well. This configuration generates OAM weight. For example, when the signal is input to IN.1, the phase difference among the four output ports is 0. When the signal is input to IN.2, the phase differences between adjacent output ports are $\frac{\pi}{2}$. Note that this circuit also equally distributes the power at any input ports among all output ports. Although the structure of the DFT network may become complex when realized, a broadband network can be realized without an excessive increase in hardware cost because the there are many techniques for realizing broadband hybrids, for example, see [12] and [13]. This is a key advantage of the analog technique over digital signal processing; the computation complexity of the latter is proportional to the signal bandwidth and so tends be excessive.

B. Proposed method

In this study, we use dual circular polarized waves and the mode selection technique. At first, we describe how dual circular polarization (CP) is incorporated into OAM transmission. The dual circular polarized waves are generated using dual-port microstrip antennas and 90 degree hybrid couplers. Figure 4 presents a dual-port microstrip antenna. The 90 degree hybrid couplers also distributes the input power equally, and the phase difference among the output ports is $\frac{\pi}{2}$. By using both input ports of the hybrid, both right hand (RH) and left hand (LH) CP are simultaneously radiated; this is a well-known technique for generating dual CP. By using this technique, the number of the available modes can be doubled without using digital processing.

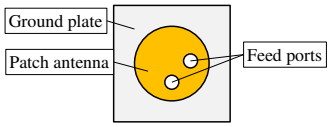

Fig. 4. Dual-port antenna.

The transmitter and receiver are assumed to have identical circular array antennas, where each array element comprises the antennas shown in Fig. 4, and the two array antennas face each other straight on. This configuration yields channel matrix $\boldsymbol{H}$, and the channel observed through the 90 degree hybrid at both sides of the array antennas is expressed as,

$$\begin{aligned} \boldsymbol{H}_{\rm c} &= \boldsymbol{W}_{90}^{H}\boldsymbol{H}\boldsymbol{W}_{90} \\ &= \begin{pmatrix} \boldsymbol{h}_{\rm co}^{\rm RR} & \boldsymbol{h}_{\rm x}^{\rm RL} \\ \boldsymbol{h}_{\rm x}^{\rm LR} & \boldsymbol{h}_{\rm co}^{\rm LL} \end{pmatrix}, \end{aligned} \tag{7}$$

where $\boldsymbol{h}_{\rm co}^{\rm RR}$ and $\boldsymbol{h}_{\rm co}^{\rm LL}$ is the channel matrix of RHCP and LHCP, respectively, and $\boldsymbol{h}_{\rm x}^{\rm RL}$ and $\boldsymbol{h}_{\rm x}^{\rm LR}$ are the channel matrices of cross CP. $\boldsymbol{W}_{90}$ is defined as,

$$\boldsymbol{W}_{90} = \frac{1}{\sqrt{2}} \begin{pmatrix} \boldsymbol{I} & \boldsymbol{w}_{90} \\ \boldsymbol{w}_{90} & \boldsymbol{I} \end{pmatrix}, \tag{8}$$

where $\boldsymbol{I}$ is an $N \times N$ identity matrix and $\boldsymbol{w}_{90}$ are diagonal matrices that contain $e^{-j\frac{\pi}{2}}$. By multiplying the weights as per (3), the channel through the weight matrices is expressed as,

$$\begin{aligned} \boldsymbol{H}_{\rm OAM} &= \boldsymbol{U}_{M}^{H}\boldsymbol{H}_{\rm c}\boldsymbol{U}_{M} \\ &= \begin{pmatrix} \boldsymbol{C}_{\rm co}^{\rm RR} & \boldsymbol{C}_{\rm x}^{\rm RL} \\ \boldsymbol{C}_{\rm x}^{\rm LR} & \boldsymbol{C}_{\rm co}^{\rm LL} \end{pmatrix}, \end{aligned} \tag{9}$$

where $\boldsymbol{U}_M$ is expressed as

$$\boldsymbol{U}_{M} = \begin{pmatrix} \boldsymbol{W}_{N} & \boldsymbol{0} \\ \boldsymbol{0} & \boldsymbol{W}_{N} \end{pmatrix}, \tag{10}$$

where M expresses the number of ports at each side of the array, $\boldsymbol{U}_M$ is a unitary matrix, and $\boldsymbol{W}_N$ is defined in (6). Since N represents the total number of modes for each polarization, $M = 2N$ is satisfied. Note that $N = 4$ is assumed due to the antenna configuration dealt with in this simulation study. Ideally, $\boldsymbol{C}_{\rm co}^{\rm RR}$ and $\boldsymbol{C}_{\rm co}^{\rm LL}$ are complex diagonal matrices, but imperfect antenna arrangements yield non-diagonal components that cause inter-stream interference. Ideally, $\boldsymbol{C}_{\rm x}^{\rm RL}$ and $\boldsymbol{C}_{\rm x}^{\rm LR}$ are zero matrices, but they become non-zero matrices due to inter-polarization leakage in the channel matrices $\boldsymbol{h}_{\rm x}^{\rm LR}$ and $\boldsymbol{h}_{\rm x}^{\rm RL}$. This also causes inter-stream interference. While the non-diagonal components of $\boldsymbol{H}_{\rm OAM}$ cause inter-stream interference, it can be reduced by accurate antenna arrangement and antenna elements with high cross-polarization discrimination (XPD).

Next, we will describe the mode selection method. The diagonal elements of $\boldsymbol{H}_{\rm OAM}$ are given as,

$$\mathrm{diag}(\boldsymbol{H}_{\rm OAM}) = (h_{\rm OAM11}, h_{\rm OAM22}, \cdots, h_{{\rm OAM}mm}), \tag{11}$$

where $h_{{\rm OAM}mm}$ represents the element of matrix $\boldsymbol{H}_{\rm OAM}$, and the amplitude of the diagonal components shown in (11) corresponds to the gain of the mode. The key idea of the mode selection proposal is excluding the weakest L modes, such that the maximum rate is achieved when all available power is equally distributed to all remaining modes. The easiest way to evaluate the achievable rate with several excluded modes is explained as follows. The modes are classified by using (11) as,

$$\boldsymbol{X}_{\rm sel} = \{k|\ |h_{{\rm OAM}kk}| > |h_{{\rm OAM}ll}| (l \notin \boldsymbol{X}_{\rm sel})\}, \tag{12}$$

where $l \notin \boldsymbol{X}_{\rm sel}$ corresponds to the excluded mode index. The SINR of k-th mode ($k \in \boldsymbol{X}_{\rm sel}$) is calculated by

$$\gamma(k) = \frac{\dfrac{P_0}{M-L}|h_{{\rm OAM}kk}|^2}{\dfrac{P_0}{M-L}\left\{\left(\displaystyle\sum_{i\in\boldsymbol{X}_{\rm sel}}|h_{{\rm OAM}ki}|^2\right) - |h_{{\rm OAM}kk}|^2\right\} + \sigma_n^2}, \tag{13}$$

where P_0 represents the total transmitting power and σ_n^2 represents the noise power. From equation (13), the achievable rate of the proposed method is given by,

$$C_{\rm prop.} = \sum_{k\in\boldsymbol{X}_{\rm sel}} \log_2(1+\gamma(k)). \tag{14}$$

The mode selection method determines the number of excluded modes based on the receiving gain and interference among the modes. The proposed method determines the number of excluded modes by the following steps.

1) The gains of modes and interference power among all modes are observed.
2) The relation between the number of the excluded modes, L, and achievable rate is verified, where the weakest L modes are excluded, and all available power is distributed equally to the remaining modes.
3) L with the maximum rate is identified from the results of step 2).

Note that, dual circular polarized waves are used to increase the number of streams and optimization of mode number is performed by considering all available modes.

One example is a backhaul network for cellular base-stations. The distance is much longer than the aperture width and is always constant after base-station installation. The system can constantly use the ports corresponding to the mode selected by this method, but the number of available modes may be limited. In that case, the initial computation is needed, but the cost incurred by selection is almost negligible. Another practical example is the application to vehicle platooning for self-driving cars. The vehicles may share a lot of information, e.g. the video images for collision avoidance systems and the status of the vehicle (speed, acceleration, brake). In this application, the relative distances to the neighboring vehicle are mostly constant over short periods, but the distance may vary depending to the situation, such as the road and traffic conditions. The distance can be several wavelengths (microwave band), and the propagation environment is completely line-of-sight. This means that OAM transmission is quite suitable for this scenario. In that case, a table of modes selected for inter-vehicle distance can be prepared beforehand.

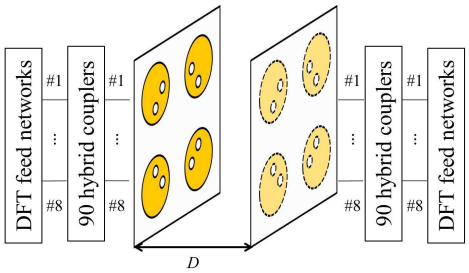

Fig. 5. System model.

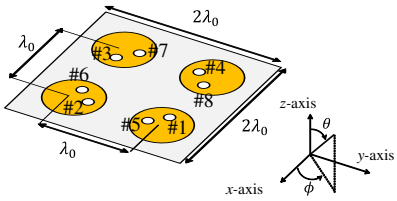

Fig. 6. Antenna model.

III. Numerical Analysis

A. Analysis condition

As described in II, OAM weight multiplication can be realized by an analog circuit. Since the feasibility of the analog DFT feed network was well studied in [5], this paper verifies the performance of OAM transmission with an ideal feed network. Focusing on the ideal feed network yields a simple evaluation of the ultimate performance of the OAM antenna configuration.

Figure 5 shows a system model. Transmitter and receiver antennas have a circular array arrangement with plane symmetry; the dual-port circular elements face each other. D is the distance between transmitter and receiver side antennas. Each antenna is connected via a 90 degree hybrid coupler to the DFT feed network.

Figure 6 shows the antennas dealt with in this paper. The permittivity and permeability of the antenna substrate are taken to be identical to that of vacuum for simplicity. Total antenna size is $2\lambda_0 \times 2\lambda_0$ (λ_0: wavelength in a vacuum). Antenna separation on the same side is λ_0. Frequency used is 2.47125 GHz. θ and ϕ are defined as shown Fig. 6.

Figure 7 plots the S-parameter from port 1 to port $1 \sim 8$. Since the antenna in this paper has point symmetry at the antenna center, we describe only the S-parameter from port 1 to the others. Note that S_{k1} represents the S-parameter from port 1 to port k. The curves show that the designed antenna array has fairly good performance at the operation frequency in terms of reflection and coupling; both are lower than -20 dB at the operation frequency (2.47125 GHz).

Figure 8 shows the actual gain of desired and cross polarized components for a single antenna element and axial ratio (AR) for a single antenna element. This result shows that the maximum level of the desired polarized waves is 9.9 dBi at $\theta = 0°$. Moreover, the half-power width is 80 degrees. Maximum level of XPD is 33 dB at $\theta = 0°$. In addition, AR

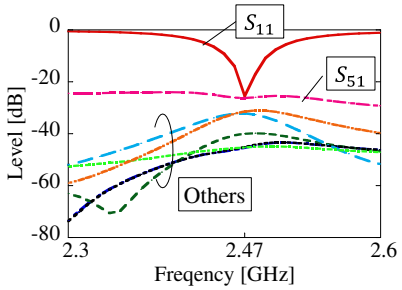

Fig. 7. S-parameter of the antenna

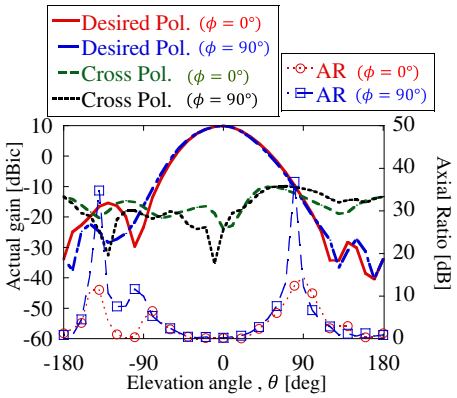

Fig. 8. Actual gain and axial ratio as functions of the elevation angle.

at $\theta = 0°$ is 0.15 dB. The angular range of the AR values under 3 dB runs from $-60° \leq \theta \leq 50°$. From Fig. 8, it is necessary to lower the isolation level in order to improve the XPD since the isolation level in the front direction of the antenna element is almost equal to the XPD.

Figure 9 shows the radiation patterns yielded by the proposed method.

Four OAM modes are realized for both polarizations. The RHCP and LHCP are simultaneously realized by setting ± 90 degree phase difference to dual-ports at each microstrip antenna. From this figure, OAM mode 0 with RHCP and LHCP has maximum gain on the z-axis. The maximum gain is 13 dBi at $\theta = 0°$, and this OAM mode for both CPs is understood as a main mode. On the other hand, the other modes do not have maximum gains on the z-axis direction. The maximum gain of OAM modes ± 1 (both polarizations) is 5.5 dBi at $\theta = 20°$. In addition, OAM mode 2 with RHCP and LHCP has 8 dBi maximum gain at $\theta = 35°$.

B. Analysis results

Figure 10 plots achievable rate versus SNR for 8×8 SR-MIMO, SR-MIMO with WF, and the proposed method. In this study, the channel capacity of SR-MIMO, C, is given by,

$$C = \log_2 \det \left(\boldsymbol{I}_M + \frac{P_0}{M\sigma_n^2} \boldsymbol{H}_{\mathrm{OAM}} \boldsymbol{H}_{\mathrm{OAM}}^H \right), \qquad (15)$$

where $\boldsymbol{I}_M$ is an $M \times M$ identity matrix. Total transmitting power, P_0, is -10dBm and noise level, σ_n^2, is -50 dBm. For the proposed method, the number of excluded modes is

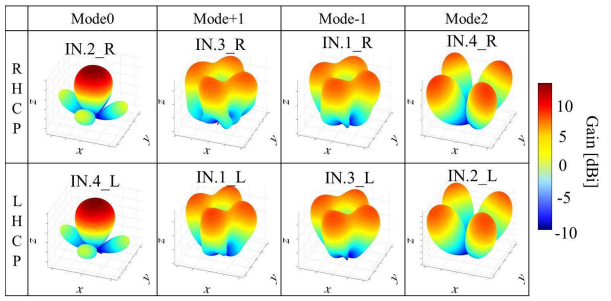

Fig. 9. Radiation pattern with OAM mode and CP. The notes above the pattern represent the index number of the excited port in the DFT matrix, e.g. IN.1_R corresponds to the port1 in Fig. 3 for RHCP.

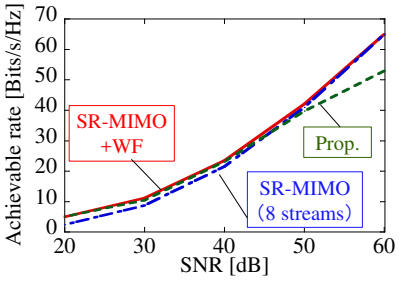

Fig. 10. Achievable rate versus SNR.

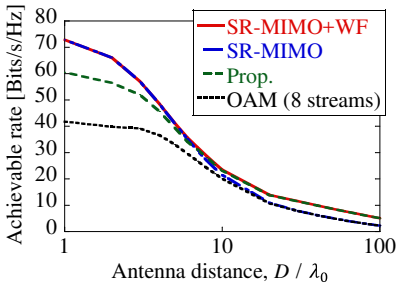

Fig. 11. Achievable rate versus antenna distance, D.

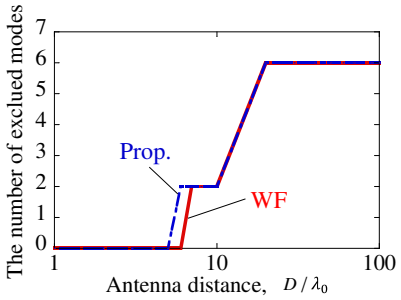

Fig. 12. The number of excluded modes, L, versus distance, D.

determined by finding the value of L that yields the maximum achievable rate. The achievable rate of OAM is given in (14) when the number of excluded modes is 0. From this figure, the difference in the curves is less than 0.5 bits/s/Hz in the range of 20 to 40 dB. However, a clear difference exists above 50 dB. In addition, SR-MIMO has greater achievable rate than the proposed method at high SNR values because the level of interference is greater than the noise power.

Figure 11 plots achievable rate versus D. In this figure, SNR is 40 dB. The results reveal that the performance of the proposed method asymptotically approaches that of SR-MIMO with WF as D increases. SR-MIMO has lower performance than the proposed method at $D = 7\lambda_0$. When $D = 100\lambda_0$, the proposed method has double the performance of SR-MIMO. Therefore, the proposed method works well even when D is larger than about $10\lambda_0$.

Figure 12 shows how the number of excluded modes changes with D for WF and proposed method. From this result, the number of excluded modes increases with D. In the area of $1\lambda_0$ to $7\lambda_0$, the number of excluded modes is 0.These results reveal that the proposed method is not effective if the distance is extremely short. This technique can be used when the distance is comparable to or longer than the aperture width. Moreover, the number is 6 for D above $20\lambda_0$. These results are almost same as the results yielded by WF. This is because arrays sufficiently distant from each other suffer from mode degeneration, i.e. only single eigen-paths can be observed due to the strong LOS environment. Since this scheme uses dual CP, only a fundamental mode generating a single beam remains for each polarization.

Next, the impact of non-ideal environments on the performance of the proposed method is studied. Essentially, the proposed method only works in LOS environments because the cyclic channel matrix cannot be realized in non-LOS (NLOS) environments. Nevertheless, the array displacement from the ideal location will affect the performance as well, even in LOS environments.

Figure 13 shows the simulation model; either of the arrays move from $x = 0$ to $10\lambda_0$, where Δx is the displacement distance in the x-axis direction. By analyzing this model, the performance of the proposed method is evaluated when the channel matrix is not a perfect cyclic matrix.

Figure 14 plots achievable rate versus the displacement distance, Δx, for SR-MIMO with 8 streams, SR-MIMO with WF, proposed method, and OAM transmission with 8 streams. This result reveals that the achievable rate with OAM transmission with 8 streams rapidly decreases in the range $0 \leq \Delta x \leq 1.5\lambda_0$. This indicates that the OAM mode is greatly affected by non-ideal antenna arrangement, and the interference among modes is increased due to the imperfect channel. On the other hand, the proposed method yields better performance even if the channel is not ideal. This means that mode selection is also effective in alleviating the inter-mode interference created by imperfect channels. In this case, the proposed method improves the achievable rate by 10 bits/s/Hz at $\Delta x = 1.5\lambda_0$ compared to the OAM transmission method using 8 streams.

Figure 15 plots the number of excluded modes versus Δx for SR-MIMO with WF and proposed method. From this result, the number of excluded modes of the proposed method is generally 6. This means that the proposed method uses the remaining 2 OAM modes that correspond to RHCP and LHCP fundamental modes.

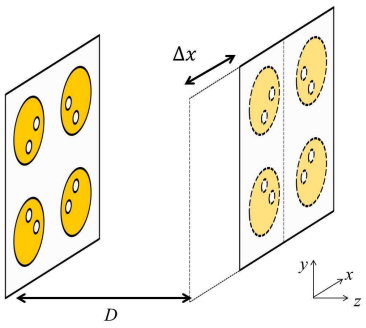

Fig. 13. The simulation model for non-ideal arrangement.

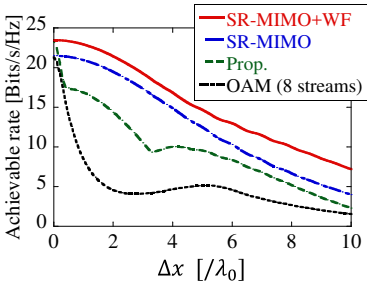

Fig. 14. Achievable rate versus Δx.

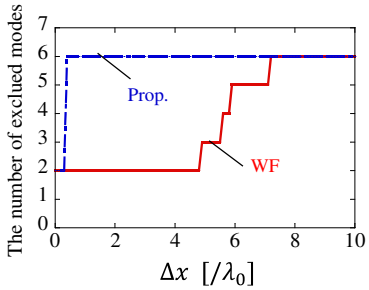

Fig. 15. The number of excluded modes versus Δx.

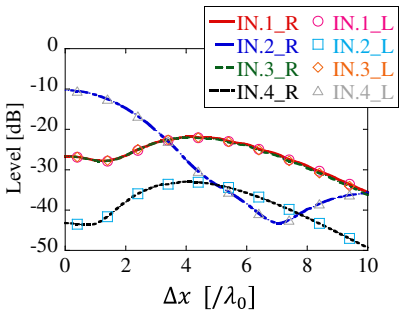

Fig. 16. The mode gains versus Δx.

Figure 16 plots mode gain versus Δx. Note that the mode gain is defined by $\mathrm{diag}(\boldsymbol{H}_{\mathrm{OAM}})$ in (11). This result reveals that there is a crossover of the first (IN.2_R/L) and second (IN.1_R/L) mode curves around $\Delta x = 3\lambda_0$ for both polarizations. This is because the first mode pattern has its gain maximum in the front direction while the second mode pattern has its gain maximum in the oblique direction.

IV. Conclusion

This paper has proposed a mode selection scheme to improve the achievable rate for OAM transmission over fixed analog OAM networks. Also, this study has dealt with optimizing the design of arrays consisting of dual circular polarized microstrip antennas, which are suitable for OAM transmission. Analyses showed that the achievable rate of this scheme approached that of SR-MIMO with WF at antenna separation distances, D, larger than $10\lambda_0$. The proposed method offers twice the performance of SR-MIMO at $D = 100\lambda_0$. These results confirm that the proposed method is a practical way of increasing the achievable rate for OAM transmission over fixed analog DFT networks.

References

[1] J. S. Jiang and M. Ingram, "Spherical-wave model for short-range MIMO," IEEE Transactions on Communications, vol. 53, no. 9, pp. 1534-1541, 2005.

[2] K. Nishimori, N. Honma, T. Seki and K. Hiraga, "On the transmission method for short-range MIMO communication," IEEE Transactions on Vehicular Technology, vol. 60, no. 3, pp. 1247-1251, 2011.

[3] I. Sarris and A. Nix, "Design and performance assessment of high-capacity MIMO architectures in the presence of a line-of-sight component," IEEE Transactions on Vehicular Technology, vol. 56, no. 4, pp. 2194-2202, 2007.

[4] O. Edfors and A. Johansson, "Is orbital angular momentum (OAM) based radio communication an unexploited area?," IEEE Transactions on Antennas and Propagation, vol. 60, no. 2, pp. 1126-1131, 2012.

[5] K. Murata, N. Honma, K. Nishimori, N. Michishita and H. Morishita, "Analog eigenmode transmission for short-range MIMO based on orbital angular momentum," IEEE Transactions on Antennas and Propagation, vol. 65, no. 12, pp. 6687-6702, 2017.

[6] Z. Li, Y. Ohashi and K. Kasai, "A dual-channel wireless communication system by multiplexing twisted radio wave," The 44th European Microwave Conference, pp. 235-238, 2014.

[7] B. Palacin, K. Sharshavina, K. Nguyen and N. Capet "An 8x8 butler matrix for generation of waves carrying orbital angular momentum (OAM)," The 8th European Conference on Antennas and Propagation (EuCAP), pp. 2814-2818, 2014.

[8] K. Murata, N. Honma, K. Nishimori, D. Klymyshyn and H. Morishita, "Four-stream parallel transmission for short-range MIMO using only passive analog components," IEICE Transactions on Communications, vol. 99, no. 1, pp. 69-80, 2016.

[9] B. Liu, Y. Cui and R. Li, "A broadband dual-polarized dual-OAM-mode antenna array for OAM communication," IEEE Antennas and Wireless Propagation Letters, vol. 16, pp. 744-747, 2017.

[10] X. Bai, X. Liang, Y. Sun, P. Hu, Y. Yao, K. Wang, J. Geng and R. Jin, "Experimental array for generating dual circularly-polarized dual-mode OAM radio beams," Scientific Reports, vol. 7, no. 1, 2017.

[11] K. Yuri, N. Honma and M. Sasaki, "Evaluation of analog OAM transmission using dual-circular polarized antenna array," 2017 International Symposium on Antennas and Propagation, POS3-1224, Oct. 2017.

[12] S. Gruszczynski and K. Wincza, "Broadband 4 × 4 Butler matrices as a connection of symmetrical multisection coupled-line 3-dB directional couplers and phase correction networks," IEEE Transactions on Microwave Theory and Techniques, vol. 57, no. 1, pp. 1-9, 2009.

[13] B. Liu, Y. Cui and R. Li, "A broadband dual-polarized dual-OAM-mode antenna array for OAM communication," IEEE Antennas and Wireless Propagation Letters, vol. 16, pp. 744-747, 2017.